Nitrogen-Doped Carbon Nanotubes as Platinum Catalyst Supports for Oxygen Reduction Reaction in Proton Exchange Membrane Fuel Cells

Drew C. Higgins,[†] Doralice Meza,[†,‡] and Zhongwei Chen*[,†]

Department of Chemical Engineering, Waterloo Institute of Nanotechnology, Waterloo Institute for Sustainable Energy, University of Waterloo, 200 University Avenue West, Waterloo, Ontario, Canada, N2L 3G1, and Department of Chemistry, Universidad Autonoma Metropolitana—Iztapalapa, Avenida San Rafael Atlixco 186, Mexico City, Mexico, 09340

Received: July 21, 2010; Revised Manuscript Received: November 1, 2010

Nitrogen-doped carbon nanotubes (N-CNTs) were utilized as platinum nanoparticle support materials, with the significant effect of the nitrogen precursor solution utilized N-CNT growth elucidated. N-CNTs synthesized from a nitrogen-rich ethylenediamine (ED) precursor solution (ED-CNTs) were found to have superior catalytic activity toward the oxygen reduction reaction (ORR) compared with N-CNTs grown from a precursor solution with relatively low nitrogen content pyridine (Py-CNTs). Significant increase in the nitrogen incorporation and edge plane exposure was observed for ED-CNTs. When utilized as platinum nanoparticle supports, Pt/ED-CNTs displayed significantly enhanced electrocatalytic activity toward the ORR when compared with Pt/Py-CNTs and nitrogen free Pt/CNTs, with the increase in performance being attributed to the distinct structural and electronic enhancements resulting from heterogeneous nitrogen doping. The performance of Pt/ED-CNTs as a cathodic catalyst for proton exchange membrane fuel cell operation was found to be significantly higher than that of Pt/CNT.

1. Introduction

Proton exchange membrane (PEM) fuel cells are considered to be a favorable alternative energy source for future generations due to their high performance efficiency and low environmental impacts.[1−4] Significant hindrance on the large scale commercialization is observed however due to the large cost of component materials, mainly, the catalyst required on the cathode for the oxygen reduction reaction (ORR).[3,5] ORR limitations are one of the main challenges with respect to fuel cell performance, as ORR catalysts suffer from high overpotential, slow kinetics, and low durability under operating conditions.[3,6] Platinum (Pt) nanoparticles supported on carbon black (Pt/C) is currently the accepted catalyst material;[7−10] however, to realize the commercialization of low temperature fuel cells, the significant Pt requirement must be reduced. This can potentially be achieved by developing nanostructured platinum catalyst materials with increased activity and utilization.[3,11,12]

Carbonaceous materials are the preferred catalyst support because they possess the essential properties of high surface area to volume ratios, good electrical conductivity, stability, and low cost.[3] It has been found that the catalytic activity of Pt nanoparticles toward ORR is strongly related to the structural and electronic properties of the carbon support material,[1,13] thus investigating potential alternative support materials could serve to increase the utilization and activity of Pt. Carbon nanotubes (CNTs) have been considered as Pt catalyst supports (Pt/CNTs) and have consistently been found to display higher catalytic activity than traditional Pt/C due to their distinct electronic and structural properties;[4,6,7,9,13−18] however, CNTs possess very low inherent catalytic activity toward the ORR. Nitrogen-doped carbon nanotubes (N-CNTs) have recently been reported to have significant catalytic activity toward ORR in alkaline conditions.[19] This ORR activity, along with the morphology and properties of the N-CNT materials is directly related to the type of nitrogen−carbon precursor and growth catalyst utilized.[20,21] Furthermore, N-CNTs synthesized from pyridine,[22] melamine,[23] and acetonitrile[24] precursor solutions have been previously investigated as platinum catalyst support materials (Pt/N-CNTs), which have been shown to display high catalytic activity and durability toward ORR in acidic conditions. This enhanced electrocatalytic activity was attributed directly to the incorporation of nitrogen into the graphitic structure of CNTs, resulting in enhanced structural and electronic properties. However, the effect of the nitrogen−carbon precursor solution utilized for N-CNT synthesis on the ORR catalytic activity of Pt/N-CNT composite materials is still not clear.

In the present study, N-CNTs synthesized from ethylenediamine (ED-CNTs) and pyridine (Py-CNTs) were utilized as Pt nanoparticle support materials in order to elucidate the effect of N-CNT precursor solution on the morphology, nitrogen content, and resulting ORR electrocatalytic activity of Pt/N-CNT composites. With comparison made to Pt/CNT materials, we demonstrate enhanced ORR activity of Pt/N-CNTs materials, with ED-CNT displaying the highest activity, directly attributed to the significant nitrogen content obtained. These highly active Pt/ED-CNTs were then utilized as a cathode catalyst in a membrane electrode assembly (MEA) and shown to have significantly higher activity than nitrogen free CNT supported Pt (Pt/CNTs) catalysts.

2. Experimental Methods

2.1. Synthesis of N-CNTs. Prefunctionalized CNTs were purchased from Nanocyl, whereas N-CNTs were synthesized using a simplistic single-injection chemical vapor deposition

* To whom correspondence should be addressed. E-mail: zhwchen@uwaterloo.ca.
[†] University of Waterloo.
[‡] Universidad Autonoma Metropolitana—Iztapalapa.

10.1021/jp106814j
Published on Web 11/24/2010

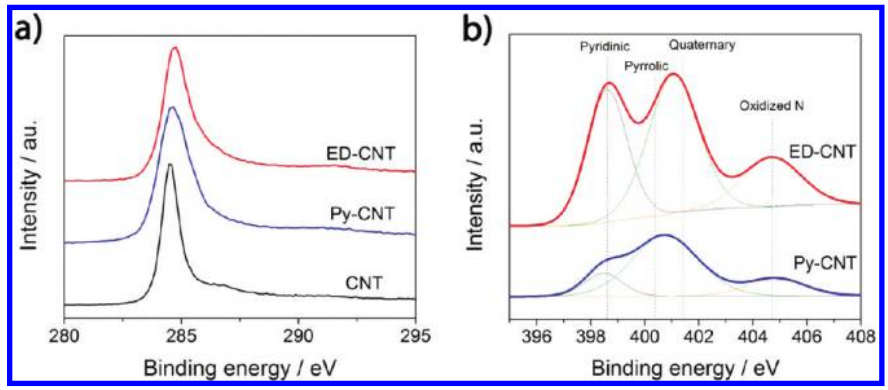

Figure 1. XPS images of (a) C1s signal displaying graphitic peaks for all samples and (b) N1s signal for ED-CNTs and Py-CNTs highlighting contributing nitrogen species.

(CVD) system, utilizing ferrocene (2.5 wt %) as a growth catalyst dissolved in either ethylenediamine or pyridine as an N-CNT source solution. Synthesis was carried out at 800 °C under inert gas flow and steady source solution injection in a horizontal quartz tube reactor chamber fitted with smaller quartz tubes as growth substrates. After the reaction was allowed to proceed, the reactor chamber was cooled to 400 °C, and air was emitted in order to burn off any amorphous carbon species. Finally, N-CNT materials were collected by scraping off the soot deposits on the growth substrates.

2.2. Deposition of Platinum Nanoparticles. Pt nanoparticle loading of synthesized N-CNTs and commercial CNTs was carried out using an ethylene glycol based method for the reduction of chloroplatinic acid hexahydrate, similar to a previous report.[13] Reduction was carried out under alkaline conditions at 140 °C for several hours. The samples were then filtered, washed, and dried overnight before collection. Pt loading was 20 wt % for all samples.

2.3. Physical Characterization. X-ray photoelectron spectroscopy (XPS) was carried out using a monochromatic Al Kα X-ray source in order to determine atomic compositions and provide insight into the atomic arrangement of the catalyst support materials. Transmission electron microscopy (TEM) was used to provide high resolution images of the catalyst materials in order to investigate the microstructure and dispersion of platinum nanoparticles. Finally, X-ray diffraction (XRD) was utilized in order to investigate the diffraction patterns of the composite catalyst materials and calculate the mean platinum nanoparticle size applying the Scherrer equation to the observed Pt(220) peak.

2.4. Electrochemical Characterization. To investigate the ORR catalytic activity of the samples, a Pine bipotentiostat rotating disk electrode (RDE) setup was used. A glassy carbon disk working electrode was loaded with a prepared catalyst ink (4 mg of catalyst material/2 mL of ethanol and deionized water). Ink (20 μL) was deposited on the electrode surface and allowed to dry, leading to a catalyst loading of 0.2 mg cm^{-2}. Then, 10 μL of a 0.05 wt % Nafion solution was applied in order to adhere the catalyst materials to the electrode surface. The catalyst loaded working electrode was immersed into a glass cell containing 0.1 M $HClO_4$ electrolyte. A platinum wire counter electrode and a Ag/AgCl reference electrode were utilized, and all potentials in acidic conditions were converted to the reference hydrogen electrode (RHE) scale for convenience. Cyclic voltammetry (CV) testing was carried out on the catalyst loaded electrode in order to determine the electrochemical surface area (ECSA) based on the hydrogen desorption charge transfer. Half cell electrochemical activity was determined by obtaining steady state linear sweep voltammetry readings under oxygen saturated and nitrogen saturated conditions as an ORR behavior and background reading, respectively. Current density polarization curves were obtained at various electrode rotation speeds.

2.5. MEA Fabrication. The performance of the Pt/ED-CNT and Pt/CNT materials as an ORR cathodic catalyst in a fuel cell setup was determined using a single cell MEA setup fabricated using a decal method as described elsewhere.[25] Briefly, catalyst ink was prepared by mixing a catalyst sample with 5% Nafion solution for 1 h. Glycerol was subsequently added, and the solution was stirred for 24 h. After preparation, the catalyst ink was painted on to decal Teflon blanks and dried in an oven. This process was repeated until the desired catalyst loading was achieved. A Nafion 112 PEM was cleaned and boiled in a dilute NaOH solution in order to ion exchange the membrane to Na^+, which allows the membrane to be hot pressed at high temperatures. After rinsing, the PEM was dried by hot pressing and then cooled prior to MEA fabrication. To load the catalyst layer onto the PEM, the decals painted with catalyst ink were pressed onto either side of the membrane and hot pressed at 210 °C and 110 lbs cm^{-2} for 5 min. Decals could then be removed, leaving the catalyst layers firmly attached to the PEM surface. The MEA was assembled into the fuel cell hardware for testing. Catalyst loading was 0.2 mg_{Pt} cm^{-2} for the cathode (Pt/ED-CNTs or Pt/CNTs) and anode (commercial Pt/C, E-TEK) and gas flow rates of 0.2 and 0.5 L min^{-1} were used for oxygen and hydrogen, respectively.

3. Results and Discussion

The successful incorporation of nitrogen in the N-CNTs was confirmed by XPS analysis and determined to be 4.74 and 2.35 at % for ED-CNTs and Py-CNTs, respectively. C1s signals for ED-CNT, Py-CNT, and CNT samples are displayed in Figure 1a. The C1s signal for CNTs displays a peak at a binding energy (BE) of 284.5 eV, very similar to the expected value of 284.3 eV for graphitic materials.[26] The C1s signal for N-CNTs exhibits a slight shift to a higher BE of and 284.8 eV for ED-CNTs and 284.7 eV for Py-CNTs, while also displaying broadened, asymmetric behavior. These are all traits which are commonly observed for N-CNT materials.[2,27,28]

The N1s signal obtained for ED-CNTS and Py-CNTs displayed in Figure 1b was broken down into three contributing peaks and analyzed in order to determine the type of nitrogen functionalities present in our samples as summarized in Table 1. The first peak, observed at a BE of 404.7 eV can be attributed to the presence of oxidized nitrogen species.[26] The second peak, located at a BE of 401.0 eV can be further broken down into two contributing species, pyrrolic nitrogen (400.0−400.6 eV) and quaternary nitrogen (401.1−401.7 eV).[26] Most importantly

TABLE 1: Nitrogen Functional Groups Present in ED-CNTs and Py-CNTs and Their Atomic Percent of Nitrogen Atoms Scanned[a]

	ED-CNT	Py-CNT
functional group	N at %	N at %
oxidized N	19.00	16.96
pyrrolic/quaternary	45.91	68.20
pyridinic	35.09	14.83

[a] ±0.01 N at %.

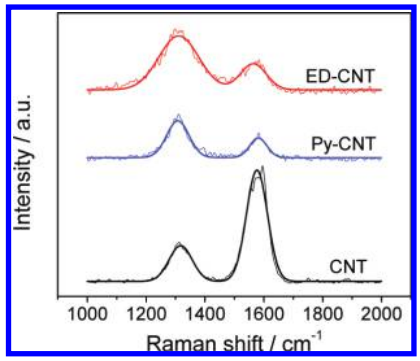

Figure 2. Raman spectroscopy for ED-CNTs, Py-CNTs, and CNTs displaying Raman first-order D and G bands.

is the third peak observed, centered at a BE of 398.6 eV, which can be directly attributed to the presence of pyridinic nitrogen species.[2,26,29] Pyridinic nitrogen atoms are heterogeneously bonded to two adjacent carbon atoms in the graphene lattice of CNTs. Because of their heterogeneous bonding nature, pyridinic nitrogen species cause structural deformations in the N-CNT samples and will expose planar edges or defect sites where they reside. Mixed reports have attributed the catalytically active sites of N-CNTs to either the pyridinic nitrogen site itself, possessing a localized electron pair, or to the planar edges and defect sites caused by the presence of these species.[2,26,29] Regardless, it has been determined that the amount of pyridinic nitrogen observed in the catalyst sample provides indication of the amount of edge plane exposure. This increase in edge plane exposure has been directly linked to the ORR performance observed, attributed to the ability of edge plane sites to readily facilitate the adsorption of oxygen, which has been directly linked to the ORR performance observed.[2,30,31] In our ED-CNT sample, pyridinic species accounted for 35.09% of the nitrogen atoms scanned, whereas in Py-CNTs this species accounted for 14.83% of the nitrogen atoms scanned. This is consistent with previous results indicating that at higher overall nitrogen contents, the formation of pyridinic functionalities is favored,[21,32] where ED-CNTs contain a significant higher overall nitrogen content compared with Py-CNTs. This increase in nitrogen content has been attributed to the higher nitrogen to carbon ratio present during synthesis due to the fact that each ethylenediamine precursor molecule has one nitrogen atom for each carbon, whereas pyridine has only one nitrogen atom for every five carbons.

Raman spectroscopy as displayed in Figure 2 was carried out in order to gauge the degree of structural deformations present in the ED-CNT, Py-CNT, and CNT samples. Two distinct peaks were observed for all samples. The D band, observed at approximately 1311 cm^{-1} for our samples, is disorder induced, being attributed to structural defects on the graphitic plane of CNTs.[28,33] The G band, observed at approximately 1581 cm^{-1}, is commonly observed for all graphitic structures and attributed to the E_{2g} vibrational mode present in the sp^2 bonded graphitic carbons.[33−35] The intensity ratio of the

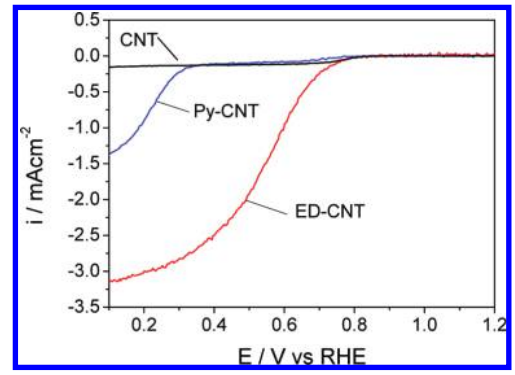

Figure 3. ORR polarization curves for pristine ED-CNTs, Py-CNTs, and CNTs in oxygen saturated 0.1 M $HClO_4$, at a scan rate of 10 mV s^{-1} in the cathodic direction at a rotation speed of 900 rpm.

first peak to the second peak, namely, the I_D/I_G ratio, provides indication of the amount of structural defects present in the catalyst support materials and provides a quantitative measure of edge plane exposure.[27,35] ED-CNTs were found to have the highest I_D/I_G ratio of 2.07, slightly higher than 1.87 for Py-CNTs and significantly larger than 0.34 observed for CNTs. The larger I_D/I_G ratios observed for N-CNTs is a result of the structural defects and edge plane exposure caused by heterogeneous nitrogen atom incorporation into the graphite layers present on the walls of N-CNTs, consistent with XPS results.

Prior to Pt loading, the electrochemical activity of pristine ED-CNTs, Py-CNTs, and CNTs toward the ORR was investigated in acidic conditions. Their respective polarization curves at 900 rpm are displayed in Figure 3. Pristine N-CNTs displayed significant catalyst activity compared with the very limited activity observed for CNTs. This ORR activity was displayed at relatively high overpotentials as commonly observed with non-noble electrocatalyst materials.[36] The observed activity of the N-CNTs is directly attributed to the effect of nitrogen incorporation into the graphitic structure of CNTs. This has been shown to enhance the electronic and structural properties of the materials resulting in electron donor behavior[3,24,37,38] and n-type semiconductance,[28] factors that will serve to facilitate the ORR. Moreover, the performance of ED-CNTs was found to be superior to that of Py-CNTs. This can be attributed to the increase in nitrogen content, a parameter directly related to the effect of precursor solution utilized. It is proposed that the utilization of nitrogen-rich ethylenediamine for N-CNT synthesis dictates the significant nitrogen incorporation observed for ED-CNTs. A higher presence of pyridinic nitrogen was confirmed by XPS analysis, providing reasonable explanation for the enhanced ORR activity observed.[2,30,31,39]

For N-CNT and CNT support materials, surface functional groups are required in order to anchor Pt nanoparticle deposition. Pt ions will interact with the functional group on the nanotube surfaces and will subsequently be reduced, forming nucleation sites that will facilitate nanoparticle growth.[13,40,41] The presence of inherent nitrogen functional groups in ED-CNTs and Py-CNTs provide anchoring sites for the adsorption of platinum ions and subsequent nanoparticle growth[42] with the steps and proposed mechanism[43] as depicted in Figure 4. It has been proposed that chemically reactive pyridinic and quaternary surface nitrogen species provide an affinity for metal deposition,[44] resulting in successful metal particle attachment without requiring any surface functionalization procedure prior to deposition onto N-CNTs.[24,44] On the other hand, CNTs require exposure to a surface functionalization procedure,[15,35,45] which was carried out prior to purchase. This process is a necessity

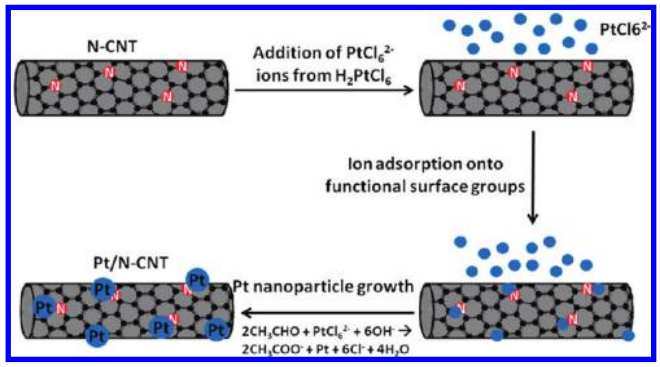

Figure 4. Schematic of ethylene glycol based platinum deposition on the surface of N-CNTs under alkaline conditions.

prior to platinum deposition in order to provide anchoring sites for platinum ion adsorption on the relatively inert surface of CNTs.[46] After platinum deposition, TEM images were taken to investigate and confirm the loading of Pt nanoparticles onto the support materials.

Figure 5 displays TEM images of Pt/ED-CNTs, Pt/Py-CNTs, and Pt/CNTs (20% wt. Pt) prior to and after platinum deposition, along with their respective particle size histograms. ED-CNTs and Py-CNTs clearly display a bamboolike structure, consistently observed with N-CNTs due to the incorporation of nitrogen atoms into the graphitic structure of the materials.[3,26,32,33,47,48] ED-CNTs (Figure 5a) display the highest degree of structural defects with smaller, rounder, bamboolike compartments, consistent with Raman analysis, whereas Py-CNTs (Figure 5c) display longer, more rectangular bamboolike compartments. CNTs (Figure 5e) as expected, display a long, tubular morphology. After platinum

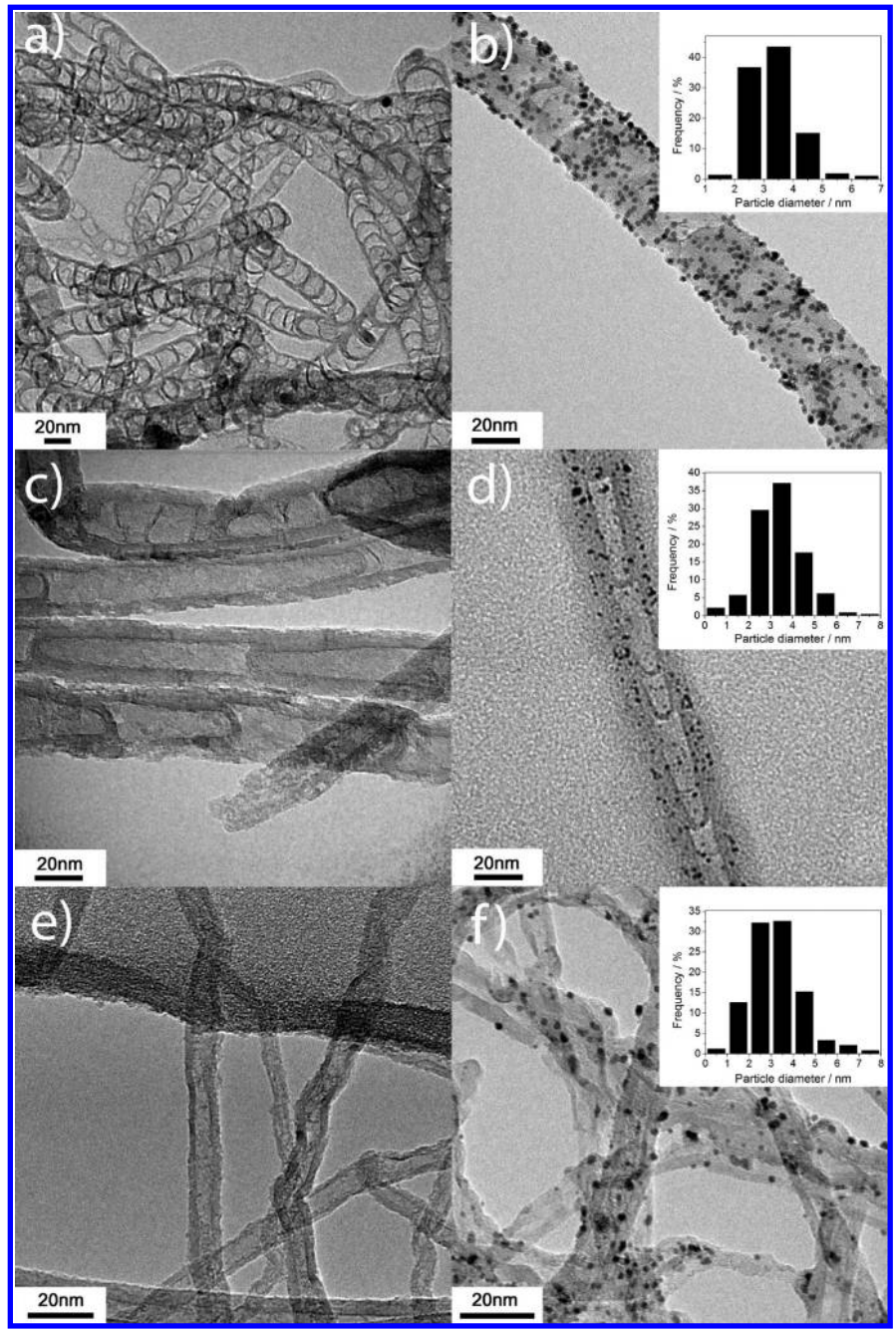

Figure 5. TEM images of (a) ED-CNTs, (b) Pt/ED-CNTs, (c) Py-CNTs, (d) Pt/Py-CNTs, (e) CNTs, and (f) Pt/CNTs along with the corresponding particle size histograms based on measurement of over 200 Pt nanoparticles.

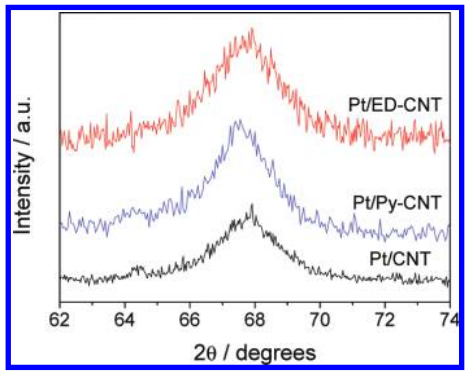

Figure 6. XRD patterns of the Pt(220) peak for Pt/ED-CNTs, Pt/Py-CNTs, and Pt/CNTs.

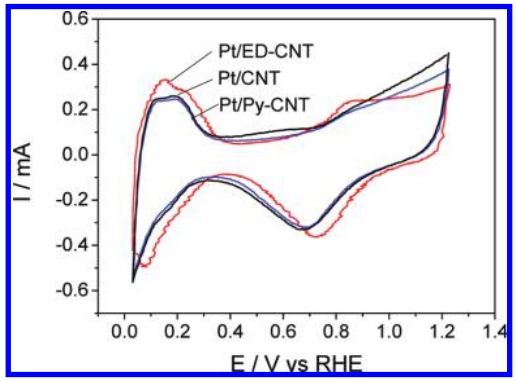

Figure 7. CV curves for Pt/ED-CNTs, Pt/Py-CNTs, and Pt/CNTs in nitrogen-saturated 0.1 M $HClO_4$ at a scan rate of 50 mV s^{-1}.

deposition, Pt/ED-CNTs (Figure 5b) display the best dispersion of uniformly sized platinum nanoparticles. Pt/Py-CNTs (Figure 5d) display well-dispersed platinum nanoparticles with a relatively higher degree of nonuniformity in the particle sizes observed. Pt/CNTs (Figure 5f) display the highest degree of nonuniform particle sizes compared with the other samples.

XRD patterns of the Pt(220) peak are displayed for each sample in Figure 6. Average platinum nanoparticle sizes were calculated for each sample by applying the Scherrer equation[13,40] and found to be 3.73 nm for Pt/ED-CNTs, 4.06 nm for Pt/Py-CNTs, and 4.09 nm for Pt/CNTs. The difference in average platinum nanoparticle size was attributed to the number of functional sites available on the surface of the support material available for platinum anchorage and nanoparticle deposition. ED-CNTs, because of their high inherent nitrogen content, possess a significant number of functional sites as confirmed by XPS analysis, leading to the reduced average platinum nanoparticle size. Relatively low nitrogen-rich Py-CNTs and nitrogen-free functionalized CNTs however possess a lower number of surface functional groups, leading to an increase in the observed average platinum nanoparticle sizes. Clearly, N-CNTs can serve to improve the deposition of Pt nanoparticles in the absence of a costly and time-consuming surface functionalization procedure that was carried out on the undoped CNTs prior to purchase. The magnitude of this improvement is directly related to the presence of inherent surface nitrogen functionalities prior to deposition.

CV cycles displayed in Figure 7 were used to determine the ECSAs of Pt/ED-CNT, Pt/Py-CNT, and Pt/CNT catalyst samples based on the charge transfer for hydrogen desorption by the following equation[49]

$$\mathrm{ECSA} = \frac{Q_{\mathrm{H}}}{mc} \quad (1)$$

where Q_{H} is the charge transfer for hydrogen desorption, m is the mass loading of Pt on the electrode, and c is the charge required to oxidize a monolayer of hydrogen on Pt (0.21 mC cm^{-2}). The ECSA for Pt/ED-CNTs was calculated to be 67.5 $m^2\ g^{-1}$, significantly higher than 38.7 and 37.7 $m^2\ g^{-1}$ calculated for Pt/Py-CNTs and Pt/CNTs, respectively. The significant increase in ECSA for Pt/ED-CNTs can be attributed primarily to the smaller average platinum nanoparticle size and the uniform particle dispersion. The ECSA is a very important parameter when dealing with electrocatalyst materials; thus CV analysis indicated Pt/ED-CNTs offer superior performance as an ORR electrocatalyst when compared with Pt/Py-CNTs containing a relatively low nitrogen content, along with nitrogen free Pt/CNTs.

Steady-state ORR polarization curves obtained for Pt/ED-CNT, Pt/Py-CNT, and Pt/CNT catalyst samples by half cell testing in an acidic electrolyte are displayed in Figure 8a. All three samples displayed significant ORR activity along with well-defined control regions (kinetic, mixed, and diffusion limited) as expected with platinum-containing materials. Pt/ED-CNTs displayed superior ORR activity compared with Pt/Py-CNTs and Pt/CNTs with respect to both half-wave potential and diffusion-limited current densities. The half-wave potential was found to increase with nitrogen content of the support materials, where a half-wave potential of 0.74 V was observed for Pt/CNTs, 0.76 V for Pt/Py-CNTs, and 0.79 V for Pt/ED-CNTs. The increase in ORR activity of the Pt-loaded N-CNTs is not as significant in magnitude compared with the pristine samples displayed in Figure 3. The ORR activity of the pristine materials derives from catalytically active N−C sites as previously mentioned, whereas improvements of the ORR activity after Pt loading mainly result from the specific Pt-support interactions and properties. Thus, the increase in ORR activity of the Pt/N-CNT composites may be attributed to several factors. Well-dispersed uniform-sized platinum nanoparticles were observed through TEM analysis, with the effect on the observed ECSA of the samples previously mentioned, factors important for the ORR electrocatalysis. Improved electronic conductivity is also reported for N-CNT materials due to the *n*-type behavior, which can serve to facilitate the facile transfer of electrons to reaction sites resulting in higher ORR reactivity.[3,22,28] A synergistic effect may also be observed between the platinum nanoparticles and the support material, where the N-CNT supports possess inherent catalytic activity as previously discussed that can serve to electrochemically reduce ORR byproducts and intermediates, mainly hydrogen peroxide.[30,31] Finally, it should be noted that an enhanced platinum support bond is present due to the nitrogen functionalities on the surface of N-CNTs.[3,22] This could be a result of the electron donor behavior commonly reported for N-CNTs[3,24,37,38] or due to the stronger adsorption of platinum onto N-CNTs as indicated by a recent first-principles study[38] and confirmed by experimental analysis.[23] The exact nature of the enhanced platinum-support bond is not well understood; however, the importance of nitrogen content in the support material is apparent. These results elucidate the effects of a high degree of nitrogen incorporation into the catalyst support material, reiterating the influence of the N-CNT precursor solution utilized on the activity of Pt/N-CNT composites. Nitrogen-rich Pt/ED-CNTs displayed significantly higher ORR electrocatalytic activity than Pt/Py-CNTs containing relatively fewer nitrogen groups. Both Pt/N-CNT samples however outperformed nitrogen free Pt/CNTs.

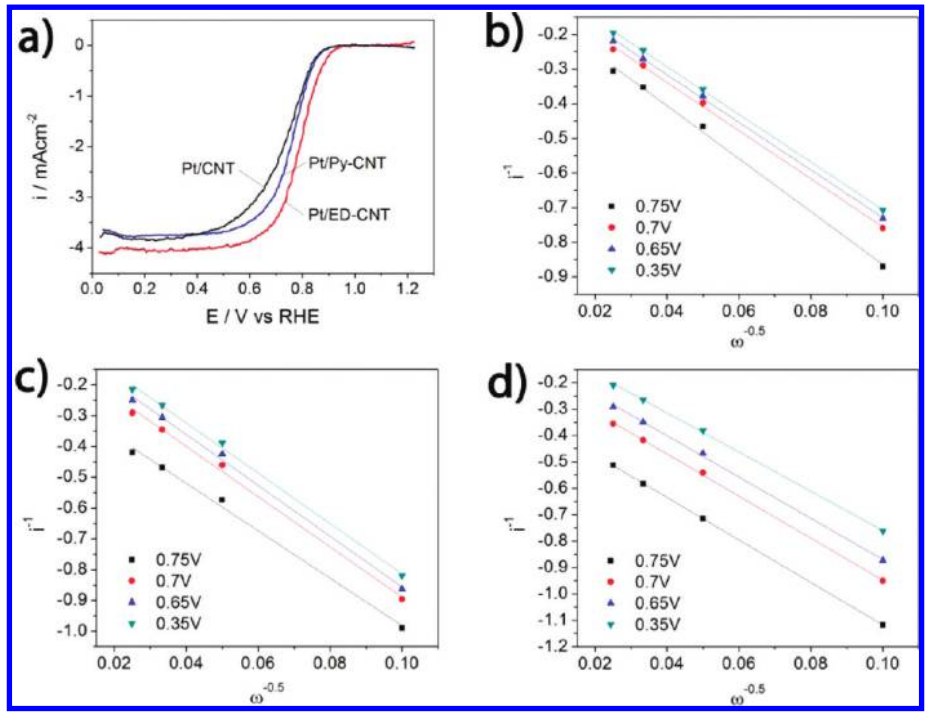

Figure 8. (a) ORR polarization curves for all samples in oxygen saturated 0.1 M $HClO_4$ at a scan rate of 10 mV s^{-1} in the cathodic direction with a rotation speed of 900 rpm after stabilization. Corresponding Koutecky−Levich plots for (b) Pt/ED-CNTs, (c) Pt/Py-CNTs, and (d) Pt/CNTs.

ORR activity in the mixed diffusion and kinetically controlled regions can be analyzed using Koutecky−Levich (KL) plots. The overall current density can be separated into the diffusion and kinetic contributions using data from different rotation speeds and applying the KL equation[50,51]

$$1/i = 1/i_k + 1/B\omega^{0.5} \quad (2)$$

where i is the observed total current density, i_k is the kinetically limited current density, ω is the rotation speed of the electrode, and B is the Levich slope which is given by the equation

$$B = 0.62nF[O_2]D_{O_2}^{2/3}\nu^{-1/6} \quad (3)$$

where n is the number of electrons transferred in the reaction, F Faraday's constant, $[O_2]$ the bulk concentration of oxygen, D_{O_2} the diffusion coefficient of oxygen, and ν the viscosity of the solution.

The right most term of the KL equation corresponds to the diffusion-limited current density, which is directly proportional to the square root of the electrode rotation speed. KL plots present the relationship of i^{-1} vs $\omega^{-0.5}$ and can be used to analyze the order of the ORR with respect to oxygen and to determine i_k values based on the intercepts. i_k values provide a good indication of the ORR kinetics on the surface of a catalyst, while eliminating the effects of reactant diffusion inside the electrochemical cell. KL plots generated for Pt/ED-CNTs, Pt/Py-CNTs, and Pt/CNTs are displayed in parts b−d of Figure 8. All three plots display linear, parallel behavior in the mixed control polarization region, indicating first-order ORR kinetics with respect to oxygen.[50] i_k values for each sample were calculated at 0.7 V vs RHE and were found to be −16.53 $mAcm^{-2}$ for Pt/ED-CNTs, −13.59 $mAcm^{-2}$ for Pt/Py-CNTs, and −6.58 $mAcm^{-2}$ for Pt/CNTs. This reiterates the importance of nitrogen content on the observed activity of the catalyst composite materials, where Pt/ED-CNTs were found to have the highest activity toward ORR after eliminating the effect of reactant diffusion.

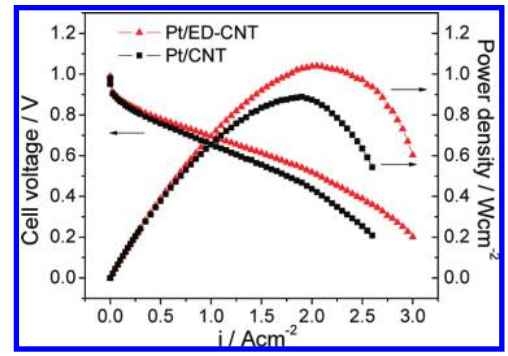

Figure 9. MEA polarization and power curves for 0.2 mg_{Pt} cm^{-2} Pt/ED-CNT and Pt/CNT cathodic catalyst loading, with 0.2 mg_{Pt} cm^{-2} commercial Pt/C as anodic catalyst in a single cell H_2/O_2 system with a Nafion 112 PEM.

Pt/ED-CNTs were selected as the optimal platinum loaded N-CNT support material due to the high observed nitrogen content leading to significant half cell activity and were subjected to testing in a MEA. Polarization and power density curves for Pt/ED-CNTs and Pt/CNTs in a single cell H_2/O_2 MEA system fabricated by a decal method are displayed in Figure 9. The peak power density for Pt/ED-CNTs was 1.04 Wcm^{-2}, an increase of approximately 16.9% over that of Pt/CNTs (0.89 W cm^{-2}). At a cell voltage of 0.6 V, Pt/ED-CNTs displayed a current density of 1.55 A cm^{-2}, approximately 24% higher than Pt/CNTs (1.25 A cm^{-2}). Concurrent with half cell electrochemical testing and cyclic voltammetry analysis, Pt/ED-CNTs display improved ORR catalytic activity compared with Pt/CNTs under fuel cell conditions.

4. Conclusions

In summary, the importance of nitrogen precursor solution utilized for the growth of N-CNTs was elucidated for their

application as platinum nanoparticle electrocatalyst support materials for the ORR. Utilization of nitrogen-rich ethylenediamine as a precursor solution produced ED-CNTs with a relatively high nitrogen content (4.74 N at %) as compared with pyridine-based Py-CNTs (2.35 N at %). This significant increase in nitrogen content led to facile deposition of well dispersed, uniformly sized platinum nanoparticles. A substantial increase in the ORR activity of these platinum composites was observed for Pt/ED-CNTs and Pt/Py-CNTs when compared with the nitrogen-free Pt/CNTs. The observed half-wave potential was found to improve with increased nitrogen content in the support material. Pt/ED-CNTs were found to display a 16.9% increase in peak power density and a 24% increase in current density at a cell potential of 0.6 V when tested in a MEA and compared with Pt/CNTs. N-CNTs are established as a potential alternative to replace traditional platinum support materials due to their distinct structural and electronic properties resulting in enhanced ORR performance. The present work highlights the importance of utilizing a nitrogen-rich N-CNT precursor solution to a high degree of nitrogen incorporation in the electrocatalyst support materials.

Acknowledgment. This work was financially supported by the Natural Sciences and Engineering Research Council of Canada (NSERC) and the University of Waterloo. TEM images were obtained at the Canadian Centre for Electron Microscopy at McMaster University.

References and Notes

(1) Maiyalagan, T.; Viswanathan, B.; Varadaraju, U. *Electrochem. Commmun.* **2005**, *7*, 905–912.
(2) Matter, P.; Zhang, L.; Ozkan, U. *J. Catal.* **2006**, *239*, 83–96.
(3) Shao, Y.; Sui, J.; Yin, G.; Gao, Y. *Appl. Catal. B* **2008**, *79*, 89–99.
(4) Wang, C.; Waje, M.; Wang, X.; Tang, J.; Haddon, R.; Yan, Y. *Nano Lett.* **2004**, *4*, 345–348.
(5) Girishkumar, G.; Vinodgopal, K.; Kamat, P. *J. Phys. Chem. B* **2004**, *108*, 19960–19966.
(6) Kongkanand, A.; Kuwabata, S.; Girishkumar, G.; Kamat, P. *Langmuir* **2006**, *22*, 2392–2396.
(7) Wang, S.; Jiang, S. P.; White, T. J.; Guo, J.; Wang, X. *J. Phys Chem. C* **2009**, *113*, 18935–18945.
(8) Wang, X.; Li, W.; Chen, Z.; Waje, M.; Yan, Y. *J. Power Sources* **2006**, *158*, 154–159.
(9) Li, W.; Wang, X.; Chen, Z.; Waje, M.; Yan, Y. *J. Phys. Chem. B* **2006**, *110*, 15353–15358.
(10) Chen, Z.; Waje, M.; Li, W.; Yan, Y. *Angew. Chem., Int. Ed.* **2007**, *46*, 4060–4063.
(11) Bing, Y.; Liu, H.; Zhang, L.; Ghosh, D.; Zhang, J. *Chem. Soc. Rev.* **2010**, *39*, 2184–2202.
(12) Shao, Y.; Liu, J.; Wang, Y.; Lin, Y. *J. Mater. Chem.* **2009**, *19*, 46–59.
(13) Li, W.; Liang, C.; Zhou, W.; Qiu, J.; Zhou, Z.; Sun, G.; Xin, Q. *J. Phys. Chem. B* **2003**, *107*, 6292–6299.
(14) Li, W.; Liang, C.; Qiu, J.; Zhou, W.; Han, H.; Wei, Z.; Sun, G.; Xin, Q. *Carbon* **2002**, *40*, 791–794.
(15) Waje, M.; Wang, X.; Li, W.; Yan, Y. *Nanotechnology* **2005**, *16*, S395–S400.
(16) Saha, M.; Li, R.; Sun, X. *J. Power Sources* **2008**, *177*, 314–322.
(17) Girishkumar, G.; Hall, T.; Vinodgopal, K.; Kamat, P. *J. Phys. Chem. B* **2006**, *110*, 107–114.
(18) Yang, J.; Goenaga, G.; Call, A.; Liu, D. *Electrochem. Solid State* **2010**, *13*, B55–B57.
(19) Gong, K.; Du, F.; Xia, Z.; Durstock, M.; Dai, L. *Science* **2009**, *323*, 760–764.
(20) Chen, Z.; Higgins, D.; Chen, Z. *Electrochim. Acta* **2010**, *55*, 4799–4804.
(21) Chen, Z.; Higgins, D.; Tao, H.; Hsu, R. S.; Chen, Z. *J. Phys. Chem. C* **2009**, *113*, 21008–21013.
(22) Vijayaraghavan, G.; Stevenson, K. *Langmuir* **2007**, *23*, 5279–5282.
(23) Chen, Y.; Wang, J.; Liu, H.; Li, R.; Sun, X.; Ye, S.; Knights, S. *Electrochem. Commmun.* **2009**, *11*, 2071–2076.
(24) Saha, M.; Li, R.; Sun, X.; Ye, S. *Electrochem. Commun.* **2009**, *11*, 438–441.
(25) Wilson, M.; Valerio, J.; Gottesfeld, S. *Electrochim. Acta* **1995**, *40*, 355–363.
(26) van Dommele, S.; Romero-Izquirdo, A.; Brydson, R.; de Jong, K.; Bitter, J. *Carbon* **2007**, *138*, 148.
(27) Maldonado, S.; Morin, S.; Stevenson, K. *Carbon* **2006**, *44*, 1429–1437.
(28) Panchakarla, L.; Govindaraj, A.; Rao, C. *ACS Nano* **2007**, *1*, 494–500.
(29) van Dommele, S.; Jong, K.; Bitter, J. *Chem. Commun.* **2006**, *2006*, 4859–4861.
(30) Maldonado, S.; Stevenson, K. *J. Phys. Chem. B* **2004**, *108*, 11375–11383.
(31) Maldonado, S.; Stevenson, K. *J. Phys. Chem. B* **2005**, *109*, 4707–4716.
(32) Terrones, M.; Terrones, H.; Grobert, N.; Hsu, W.; Zhu, Y.; Hare, J.; Kroto, H.; Walton, D.; Kohler-Redlich, P.; Rühle, M. *Appl. Phys. Lett.* **1999**, *75*, 3932–3934.
(33) Liang, E.; Ding, P.; Zhang, H.; Guo, X.; Du, Z. *Diam. Relat. Mater.* **2004**, *13*, 69–73.
(34) Nemanich, R.; Solin, S. *Phys. Rev. B* **1979**, *20*, 392–401.
(35) Wang, S.; Jiang, S.; Wang, X. *Nanotechnology* **2008**, *19*, 265601–225606.
(36) Gewirth, A.; Thorum, M. *Inorg. Chem.* **2010**, *49*, 3557–3566.
(37) Czerw, R.; Terrones, M.; Charlier, J.; Blase, X.; Foley, B.; Kamalakaran, R.; Grobert, N.; Terrones, H.; Ajayan, P.; Blau, W. *Nano Lett.* **2001**, *1*, 457–460.
(38) Li, Y.; Hung, T.; Chen, C. *Carbon* **2009**, *47*, 850–855.
(39) Matter, P.; Wang, E.; Arias, M.; Biddinger, E.; Ozkan, U. *J. Phys. Chem. B* **2006**, *110*, 18374–18384.
(40) Du, H.; Wang, C.; Hsu, H.; Chang, S.; Chen, U.; Yen, S.; Chen, L.; Shih, H.; Chen, K. *Diam. Relat. Mater.* **2008**, *17*, 535–541.
(41) Sun, C.; Chen, L.; Su, M.; Hong, L.; Chyan, O.; Hsu, C.; Chen, K.; Chang, T.; Chang, L. *Chem. Mater.* **2005**, *17*, 3749–3753.
(42) Bian, S.; Ma, Z.; Song, W. *J. Phys. Chem. C* **2009**, *113*, 8668–8672.
(43) Yang, J.; Deivaraj, T.; Too, H.; Lee, J. *Langmuir* **2004**, *20*, 4241–4245.
(44) Zamudio, A.; Elías, A.; Rodríguez-Manzo, J.; López-Urías, F.; Rodríguez-Gattorno, G.; Lupo, F.; Rühle, M.; Smith, D.; Terrones, H.; Díaz, D. *Small* **2006**, *2*, 346–350.
(45) Wang, X.; Waje, M.; Yan, Y. *Electrochem. Solid St.* **2005**, *8*, A42–A44.
(46) Lee, K.; Zhang, J.; Wang, H.; Wilkinson, D. *J. Appl. Electrochem.* **2006**, *36*, 507–522.
(47) Sumpter, B.; Meunier, V.; Romo-Herrera, J.; Cruz-Silva, E.; Cullen, D.; Terrones, H.; Smith, D.; Terrones, M. *ACS nano* **2007**, *1*, 369–375.
(48) Yang, S.; Zhao, G.; Khosravi, E. *J. Phys Chem. C* **2010**, *114*, 3371–3375.
(49) Chen, Z.; Xu, L.; Li, W.; Waje, M.; Yan, Y. *Nanotechnology* **2006**, *17*, 5254–5259.
(50) Elezovic, N.; Babic, B.; Vracar, L.; Krstaji, N. *J. Serb. Chem. Soc* **2007**, *72*, 699–708.
(51) Miyatake, K.; Omata, T.; Tryk, D.; Uchida, H.; Watanabe, M. *J. Phys. Chem. C* **2009**, *113*, 7772–7778.

JP106814J